Native extracellular matrix orientation determines multipotent vascular stem cell proliferation in response to cyclic uniaxial tensile strain and simulated stent indentation

P.S. Mathieu [a,b], E. Fitzpatrick [a,b], M. Di Luca [c], P.A. Cahill [c], C. Lally [a,b,d,*]

[a] Trinity Centre for Biomedical Engineering, Trinity Biomedical Sciences Institute, Trinity College Dublin, Dublin, Ireland
[b] Department of Mechanical, Manufacturing & Biomedical Engineering, School of Engineering, Trinity College Dublin, Ireland
[c] School of Biotechnology, Vascular Biology & Therapeutics Group, Dublin City University, Glasnevin, Dublin 9, Ireland
[d] Advanced Materials and Bioengineering Research Centre (AMBER), Royal College of Surgeons in Ireland and Trinity College Dublin, Dublin, Ireland

A R T I C L E   I N F O

A B S T R A C T

Cardiovascular disease is the leading cause of death worldwide, with multipotent vascular stem cells (MVSC) implicated in contributing to diseased vessels. MVSC are mechanosensitive cells which align perpendicular to cyclic uniaxial tensile strain. Within the blood vessel wall, collagen fibers constrain cells so that they are forced to align circumferentially, in the primary direction of tensile strain. In these experiments, MVSC were seeded onto the medial layer of decellularized porcine carotid arteries, then exposed to 10%, 1 Hz cyclic tensile strain for 10 days with the collagen fiber direction either parallel or perpendicular to the direction of strain. Cells aligned with the direction of the collagen fibers regardless of the orientation to strain. Cells aligned with the direction of strain showed an increased number of proliferative Ki67 positive cells, while those strained perpendicular to the direction of cell alignment showed no change in cell proliferation. A bioreactor system was designed to simulate the indentation of a single, wire stent strut. After 10 days of cyclic loading to 10% strain, MVSC showed regions of densely packed, highly proliferative cells. Therefore, MVSC may play a significant role in in-stent restenosis, and this proliferative response could potentially be controlled by controlling MVSC orientation relative to applied strain.

1. Introduction

Cardiovascular disease is the number one cause of death worldwide [1]. Stenting is the most common treatment for stenosed arteries, however 5–10% of all stents re-stenose [2]. In-stent restenosis is characterized by excessive cell proliferation, which may be driven by the proliferation of cells found in the media of an artery: vascular smooth muscle cells (VSMC) [3] and multipotent vascular stem cells (MVSC) [4]. VSMC have traditionally been thought to play a critical role in neointimal formation, whereby healthy, contractile VSMC transition to synthetic VSMC which proliferate and produce extracellular matrix within the intimal layer [5]. Other studies suggest that a small population of multipotent vascular stem cells (MVSC) migrate to the intimal layer and proliferate to form the neointima in carotid ligation [4].

Few studies have been done on MVSC. Recently, we demonstrated that MVSC strain avoid and align perpendicular to the direction of strain in response to uniaxial tensile strain [6]. Although VSMC reorient when allowed to rotate freely on unstructured surfaces, *in vivo,* VSMC are constrained by collagen fibers oriented parallel to the dominant direction of strain [7,8]. While medial vascular cells cannot undergo strain avoidant reorientation in a healthy *in vivo* environment, they may reorient in an environment where collagen fibers can remodel and change orientation, such as in atherosclerosis [9,10]. In mice, the development of atherosclerosis causes collagen fibers to reorient to be less circumferential in direction [9]. Atherosclerotic plaques often have a paucity of collagen fibers within the lipid core, while fibrous plaque caps show realignment of collagen fibers in the direction of the maximum principal strain [10]. Vascular interventions also change the collagen fiber arrangement within a vessel; in an animal study on transapical valve replacement, stent strut contact with the pulmonary

---

artery caused collagen fibers near the stent to align parallel to the stent struts, while leaving fibers between struts unaffected [11]. Additionally, our lab demonstrated that application of a simulated stent strut caused realignment of collagen fibers parallel to the stent strut direction [12]. These changes in collagen fiber orientation may change the direction of vascular cells' alignment, and could influence how these cells experience their strain environment. Despite MVSC being considered to play a critical role in vascular disease [13], to the authors' knowledge, no prior study has investigated the role of native fiber structure on MVSC, or how fiber structure influences the response of MVSC to strain.

The aim of this study was to investigate the response of MVSC to uniaxial tensile strain in the presence of native collagen structure, with fibers arranged either primarily in the direction of strain, or perpendicular to the direction of strain. To understand how the proliferative response to strain may indicate a role for MVSC in in-stent restenosis, we also designed a bioreactor system that simulated the loading of a single stent strut on strips of decellularized porcine carotid artery, recellularized with MVSC. This experimental setup enabled the response of MVSC to a stenting-type environment to be isolated from other vascular cell types and the contribution of MVSC to in-stent restenosis in a controlled strain environment to be more fully elucidated.

2. Materials and methods

2.1. Cell isolation and culture

Rat MVSC were isolated by explant as previously described [6] and were cultured in stem cell media containing high glucose DMEM (hgDMEM) with Glutamax (Bio-sciences), with 1% Penicillin/Streptomycin (Bio-Sciences), 1% N-2 supplement (Gibco), 2% B-27 supplement (Gibco), 20 ng/mL bFGF (Corning), 2% chicken embryo extract (ATCC), 100 nM retinoic acid (Sigma-Aldrich), 50 nM

2-mercaptoethanol (Gibco). Rat MVSC were used at p19. All animal research was carried out in accordance with the EU Directive 2010/63/EU on the protection of animals used for scientific purposes through the Health Products Regulatory Authority (HPRA) of Ireland. All procedures were approved by the University Ethics Committee in accordance with the guidelines of the Health Products Regulatory Authority (HPRA) for the Care and Use of Laboratory Animals.

2.2. Decellularized tissue

Porcine carotid arteries were dissected fresh and cryopreserved by freezing at a rate of -1 °C per minute in tissue freezing medium (TFM) composed of 0.1 M sucrose (Sigma-Aldrich) and 12.75% DMSO (VWR) in RPMI 1640 medium (Gibco). These arteries were then decellularized based on a previously determined protocol [14]. Briefly, they were perfused with 0.1 NaOH for 15 h and then rinsed in saline for 31 h. Vessels were incubated in DNAse solution for 19 h. Decellularized vessels were returned to TFM and frozen until ready for use. Vessels were cut into 5 mm × 10 mm strips for static samples or 5 mm × 15 mm strips for strained samples, which had a strain region of 10 mm length. Strips were cut either circumferentially for fibers predominantly parallel to strain direction; or axially, for fibers predominantly perpendicular to strain direction [15], (Fig. 1A). The intimal layer of the vessel was removed using fine tipped forceps to expose medial collagen fibres. Before cell seeding, strips were placed in 100% ethanol for at least 1 h, then rinsed twice in sterile deionized water and twice in sterile PBS. Strips were pinned flat (Fig. 1B) and seeded at 1.33×10^4 cells/cm². Cells were allowed to adhere for 1 h before strips were unpinned and transferred to culture for a further 3 days prior to initiating the application of strain.
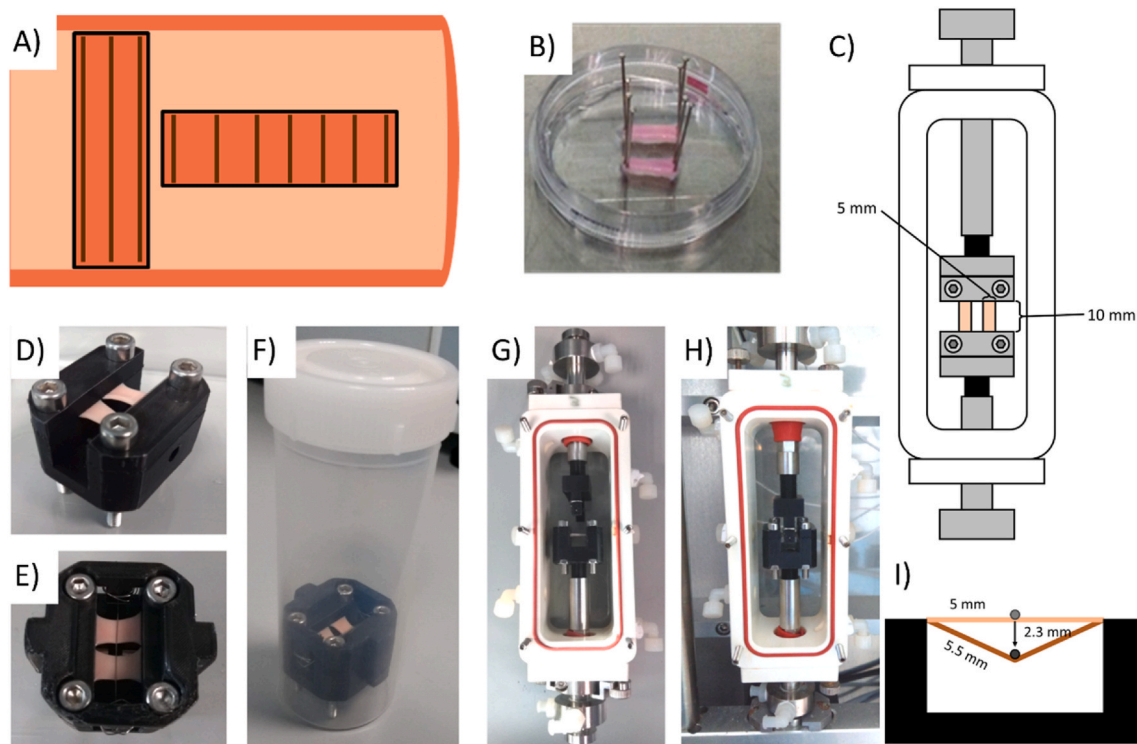

Fig. 1. (A) Diagram showing how strips were cut from decellularized porcine carotid arteries in order to obtain strips with fibers predominantly oriented parallel or perpendicular to strain direction. (B) Strips pinned for cell seeding. (C) Setup of bioreactor chambers. Images of static indentation device (D) Before application of stent strut, (E) Top view with stent strut, (F) In 120 mL tube for addition of medium. Images of the dynamic indentation device (G) with strips loaded into the Bose bioreactor chamber, and (H) loaded into the Bose Biodynamic device with stent strut placed level with the top of the recellularized strips(I)Diagram showing 10% strain of tissue strips by stent strut application.

2.2.1. Application of strain

For uniaxial tensile strain, strips were loaded into clamps within a Bose BioDynamic 5200 with two strips placed in each bioreactor chamber (Fig. 1C). Bose chambers were filled with hgDMEM with Glutamax (Bio-sciences) supplemented with 10% FBS and 2 μl/mL Primocin. A preload of 0.05 N was applied to all strips. Samples were strained uniaxially using displacement-controlled strain, from 0 to 10% strain at 1 Hz for 10 days.

For simulated stent indentation, two indentation devices were 3D printed in polylactic acid (PLA). The static device (Figs. 1D, E, F) applied a static 10% elongation of the tissue, by indenting a 250 μm wire 2.3 mm into a recellularized tissue strip. Strips were loaded into sterile rigs with two strips placed side by side (Fig. 1E). Bose chambers or tubes were filled with 10% FBS medium with 2 μl/mL Primocin. In the bioreactor, the wire indenter was allowed to rest on the surface of the strips. The wire was indented 2.3 mm into the tissue strips at 1 Hz for 10 days to apply a 10% strain to the tissue (Fig. 1I).

2.3. Staining protocol

Recellularized tissue strips were fixed for at least 24 h at 4 °C in 10% formalin. Strips were blocked and permeabilized in 5% BSA and 0.2% Triton-X 100 in PBS at room temperature for 40 min with agitation. Strips were rinsed twice in PBS. Primary antibody solution was prepared (0.5% BSA, 0.2% Triton-X 100, PBS) and antibodies were used at the concentration in Table 1. Strips were incubated in primary antibody overnight at 4 °C with agitation. Strips were rinsed three times in PBS. Secondary antibody solution was prepared (0.5% BSA, 0.2% Triton-X 100, PBS) with 1:1000 antibody, 1:500 rhodamine Phalloidin, and 1:1000 DAPI. Strips were incubated in the secondary antibody solution in the dark for 48 h at 4 °C with agitation. Strips were rinsed three times in PBS and stored at 4 °C protected from light before imaging. In indentation experiments, collagen was stained using collagen-binding adhesion protein 35 (CNA35) [16] prior to fixation. Strips were incubated in a 1:200 dilution of CNA35-dTom in the medium used for strain application at 37 °C for 2 h, then rinsed twice in PBS before fixation.

2.4. Imaging protocol

All images were taken on a Leica SP8 scanning confocal microscope at 20x. For each sample, a continuous area of at least 24 images was scanned with a z-stack taken at intervals of 10 μm. The images were taken at a 1024 × 1024 pixel resolution with a scan speed of 400 Hz.

2.5. Image analysis

ImageJ particle analysis was used to get nuclear number, nuclear orientation, major and minor axis, and nuclear area as previously described [6]. Images where nuclei were too dense to separate using particle analysis were counted. Actin alignment was determined using the MatFiber Matlab program [17] which determined the alignment of fibers in each 5 × 5 pixel region of the image. Ki67 nuclei were determined by masking Ki67 with nuclear area, and then counting positive nuclei using ImageJ particle analysis as previously described [6]. Images where Ki67+ nuclei were too dense to separate using particle analysis were counted. Immunostaining intensity measures were determined as previously described [6], then normalized to a secondary antibody control. Collagen fiber size range was determined by manually measuring the largest and smallest visibly distinct-CNA35 stained collagen fibers across multiple images of day 0 unstrained samples using the ImageJ 'Measure' function.

2.6. Statistics

Statistics were performed using GraphPad Prism 8.2.1. For experiments performed without simulated stenting, significance was determined using 2-way ANOVA with a Tukey's post-hoc test or a Sidak's post-hoc test as determined by the statistics software. When comparing across both parallel and perpendicular strain for both cell types a 3-way ANOVA was used with a Tukey's post-hoc test. Each experiment had n ≥ 3 samples. For stenting experiments, significance was determined using an ordinary one-way ANOVA for cell counts and Ki67+ nuclear counts with n ≥ 3 samples. Collagen and F-actin alignment significance was determined using a 2-way ANOVA with a post-hoc Tukey test with n ≥ 3 samples.

3. Results

For rMVSC seeded on decellularized tissue strips, application of 10%, 1 Hz uniaxial tensile strain for ten days resulted in cells aligned with the direction of collagen fibers regardless of whether the cells were oriented parallel or perpendicular to the direction of strain. This cellular orientation was determined both by the direction of the major axis of the nuclear ellipse and by the orientation of f-actin cytoskeletal fibers (Fig. 2). There was no significant change in cell number between cells that were left unstrained, or cells that were strained either parallel or perpendicular to fiber direction for ten days (Fig. S1A). Cells were also assessed for proliferation by counting the number of Ki67 positive nuclei, indicating an actively dividing cell. Cells which were exposed to strain parallel to fiber direction showed an increased percentage of Ki67 positive nuclei compared to cells that were strained perpendicular to fiber direction (Fig. S1B).

Cells showed no significant changes in nuclear size (Fig. S1C) or nucleus circularity (Fig. S1D) in response to strain. Cells showed no significant change in calponin 1 expression in response to strain either perpendicular or parallel to fiber direction indicating no shift towards a VSMC phenotype (Fig. S2).

In the stent indentation model, circumferentially cut strips were used so that collagen was aligned primarily parallel to the direction of strain and collagen was stained to determine if stent strut loading would cause collagen reorientation. Collagen aligned primarily parallel to the direction of strain in all conditions (Fig. S3). Collagen fiber size in the day 0 unstrained samples ranged between 0.5 and 4 μm in diameter. After ten days, cell alignment was evaluated using f-actin staining of cell actin cytoskeleton. Ten days of loading with either a static or a dynamic stent strut decreased the alignment of cells parallel to the direction of the collagen fibers and strain (Fig. 3). In samples without a stent strut, cells aligned with the direction of collagen fibers (Fig. 3A). In statically and dynamically loaded samples cells aligned primarily in the direction of collagen fibers, although they showed less alignment than those without a stent strut. This is likely due to cells aligned along the stent strut, perpendicular to the direction of the collagen fibers (Fig. 3B and C). Additionally, further away from the stent, in statically loaded samples cells remained aligned with the underlying collagen fibers (Fig. 3D), while in dynamically loaded samples, some regions showed cells aligning perpendicular to the direction of strain and collagen fibers (Fig. 3E).

Cell proliferation was evaluated by cell count and the number of Ki67+ cells. While samples from day 0, and unstrained cells at day 10 had countable numbers of nuclei, and Ki67+ cells (Fig. S5), samples exposed to a static stent strut for 10 days had many frames with cell nuclei that were too dense to count (Fig. S5). Samples exposed to a dynamically loaded stent strut for 10 days had both regions of nuclei, and regions of Ki67+ nuclei that were too dense to count (Fig. S5).

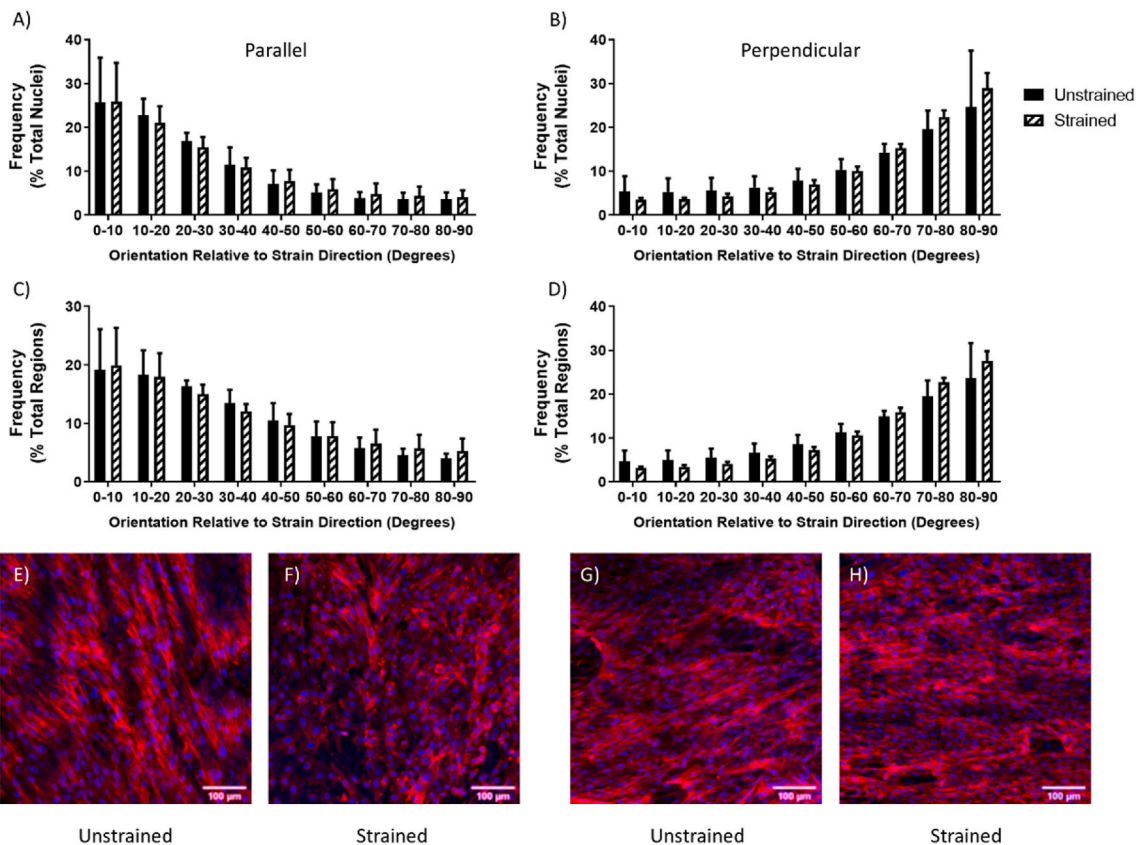Neither cell number nor percentage of Ki67+ nuclei was significantly

Table 1
Antibodies used for immunofluorescent staining.

Primary Antibodies	Concentration	Product Code
Ki67	1:200	Abcam ab15580
Calponin 1	1:100	Sigma C2687

Fig. 2. The alignment distribution of rMVSC (A,B) nuclei (C, D) and f-actin (C, D) on decellularized porcine carotid artery samples left unstrained, or (A, C) strained parallel or (B, D) perpendicular to the direction of collagen fibers. (E, F, G, H) Representative images of rMVSC on decellularized porcine carotid artery samples (E, G) left unstrained or (F) strained parallel or (H) perpendicular to the direction of collagen fibers. n = 3.

different between either of the day 0 conditions or day 10 samples that were left unstrained (Fig. 4A and B). Both day 10 conditions that involved loading with a simulated stent strut had regions where cells were too densely packed to count nuclei. The number of uncountable frames was slightly, but not significantly higher in the dynamically loaded samples than the statically loaded samples, however only dynamically loaded samples had regions where Ki67+ cells were too densely packed to count (Fig. 4C). Two out of three of the samples that were dynamically loaded had regions of densely packed and highly proliferative cells (Fig. 4D,E,F).

4. Discussion

This paper is the first to investigate the effects of structure and tensile strain on MVSC, a cell type that has been shown to play a role in intimal hyperplasia. In stenting situations, tensile strain is more complex than simple uniaxial loading. Therefore, a custom-designed rig was developed to simulate the indentation of a single stent strut. This device allowed for the generation of strains in vascular tissue like those found in an *in vivo* stenting environment.

4.1. Alignment

The aligned structure of the medial layer of the decellularized artery induced both nuclear and cytoskeletal alignment in the direction of fiber alignment. While few studies on MVSC microstructural response have been performed, MVSC align in the direction of polydimethylsiloxane (PDMS) microgrooves [18]. The native collagen structure causes cell alignment similar to engineered patterned surfaces despite having a less controlled topography. Although these experiments used rat cells on porcine tissue, both species have a similar collagen structure, thus we

expect that this mismatch would not significantly impact the results [7, 19]. Therefore, these decellularized vessels can be used to prime vascular cells to align in a circumferential direction.

When exposed to strain, MVSC remained constrained by structure. The lack of strain-avoidant reorientation shows that structural cues dominate over strain cues. Because structural cues can prevent strain-induced orientation changes, tissue engineering applications can use microstructural cues to determine MVSC alignment regardless of applied strain. However, the ability of structure to influence cell response to strain may depend on the spacing of the cues provided. In VSMC, microgroove size can determine the extent that microstructural cues dominate over strain cues. VSMC on both 70 μm microgrooves and the thinnest 15 μm microgrooves showed more strain avoidant realignment than in 40 μm microgrooves [20]. This indicates that there is an optimal microgroove width in which cells will remain the most aligned, even when subjected to uniaxial tensile strain, which may indicate that there might also be an optimal spacing of collagen fibers in order to maintain MVSC alignment with the collagen fibers in response to strain.

Loading recellularized strips with a simulated stent strut also changes cell alignment. In this simulated stent loading regime, no detectable collagen reorientation occurred. Even without collagen reorientation, cell re-alignment was observed in samples that were loaded by the simulated stent strut. The cells that realigned along the length of the stent strut likely aligned due to contact guidance from the edge of the stent strut. *In vivo,* stenting causes de-endothelialization, therefore any cells that migrate to the intimal space would contact the stent strut itself, changing the cellular orientation which may change how the cells experience strain. Under dynamic stent strut indentation, some regions of cells not near the stent strut realigned perpendicular to strain direction. This is not unexpected, given that MVSC that aren't constrained by underlying microstructural cues will reorient
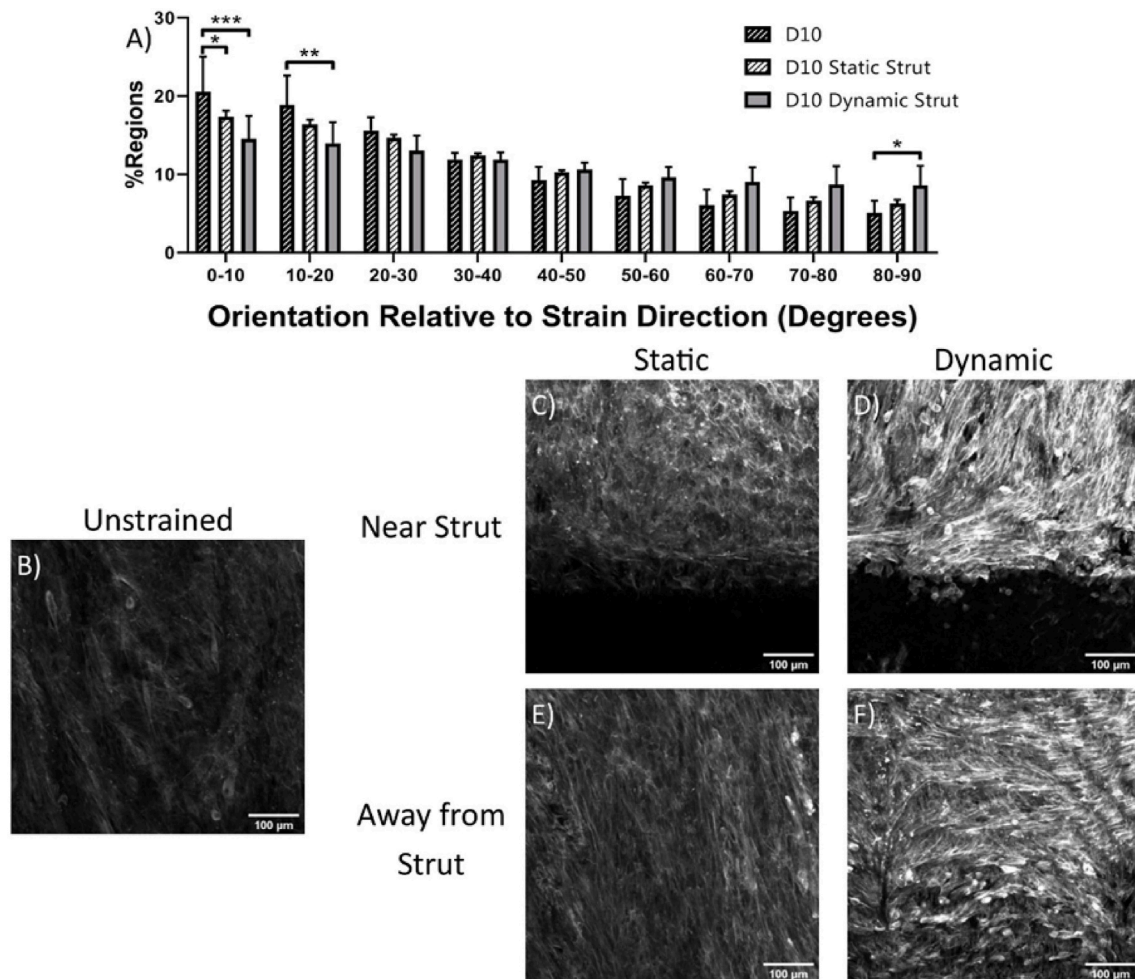
4

Fig. 3. F-actin orientation of cells exposed to various loading regimes for 10 days. (A) Stent strut indentation decreases cell alignment in strain direction. Representative images of cells stained for f-actin for (B) unstrained and (C, E) statically and (D, F) dynamically loaded cells, both (C, D) near and (E, F) far from stent strut. n = 3 Scale bar = 100 μm *p < 0.05, **p < 0.01, ***p < 0.001, ****p < 0.0001.

perpendicular to strain direction [6]. In regions where cells reoriented perpendicular to fiber and strain direction, the cells that remained in contact with the ECM structure remained oriented with the fiber direction, while the cells that had reoriented were layered over the top of other cells, so they were no longer sensing the microstructural cues from the underlying ECM. If MVSC are the primary driver of in-stent restenosis, we can anticipate that the proliferating cells would be in regions where there is ECM or other guidance causing cells to orient parallel to the direction of strain.

4.2. Proliferation and apoptosis

When exposed to strain parallel to the direction of cell alignment, the number of dividing Ki67+ MVSC increased. MVSC on unstructured substrates have shown a decrease in cell number in response to 10%, 1 Hz uniaxial cyclic tensile strain [6], however, in these experiments, cells were free to reorient and strain avoid. When MVSC were strained parallel to cell orientation, cell proliferation increased. These strain-induced changes did not appear when the cells were aligned perpendicular to the direction of strain, showing that cell orientation relative to strain direction is critical for how the cells sense uniaxial tensile strain. While cells aligned in the direction of strain increased in Ki67 nuclear localization, indicating more dividing cells, they did not significantly increase in cell number, therefore it is likely that MVSC death also increases when the cells sense strain. This would mean that they behaved similarly to VSMC which have been shown to increase in

apoptosis when exposed to cyclic tensile strain [21]. Cells appear to only sense strain when they are aligned with strain direction.

When samples were loaded with a stent strut for 10 days, both the static strut and the dynamic stent induced an increase in cell number versus unstrained samples. While static strain has not been investigated in MVSC specifically, static strain in intact vascular tissue rings showed increased DNA synthesis, possibly indicating increased cell division, in medial vascular cells [22] which could indicate the presence of MVSC in these intact tissue samples or indicate that VSMC respond differently to static strain than cyclic tensile strain. In this experiment, we see that while static strain increased MVSC proliferation, it is still qualitatively different than the proliferation seen in cyclically loaded samples.

Given the increased proliferation of MVSC when strained in the direction of cell alignment, we expected to see an increase in MVSC number when they were dynamically loaded parallel to the strain direction. When dynamically loaded, samples had regions of dense, highly proliferative cells. These areas mimic areas of in-stent restenosis which have both high cell density [23], and high proliferation [24]. This study correlates with studies of stent designs that indicate that designs that cause increased vascular strain cause increased in-stent restenosis [25–27]. The dynamic strut indentation simulates a loading environment where there is high dynamic strain applied within the artery, which would be consistent with the regions that show high in-stent restenosis.
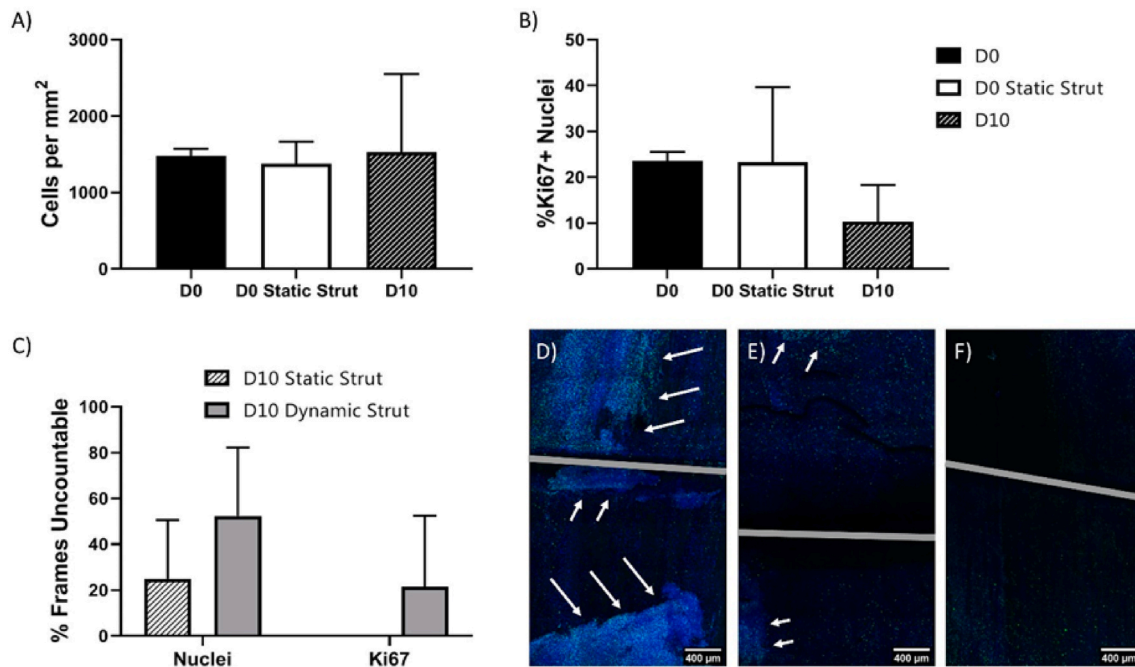
Fig. 4. Cell number and proliferation. (A) Cell number for conditions with countable nuclei. (B) Percentage of Ki67+ nuclei for conditions with countable nuclei. (C) For conditions without countable nuclei, percentage of frames for which individual nuclei or Ki67+ nuclei cannot be counted. (D–F) Images of dynamically loaded samples, with arrows pointing to regions of high density, highly proliferative cells. n = 3 Scale bars = 400 μm.

5. Conclusions

MVSC that cannot reorient, and consequently strain avoid, will proliferate when exposed to uniaxial tensile strain. Therefore, MVSC exposed to increased tensile strain could potentially over proliferate causing intimal thickening, thereby suggesting a significant role for MVSC in vascular disease, although this should be confirmed with further *in vivo* studies This research highlights the importance of cell orientation controlling vascular cell growth. When designing tissue engineered vessels or vascular interventions which change the mechanical environment in a blood vessel, it is essential to understand the strain applied to the underlying substrate, and how this strain translates to the strain sensed by the cells, which is dependent upon cellular alignment. Ultimately this alignment-directed strain sensing could be critical in understanding cell response in vascular disease. By creating a device that allows the application of both static and dynamic stent strut indentation, this paper has demonstrated that MVSC are potentially a dominant cell type in in-stent restenosis.

Declaration of competing interest

The authors declare that there are no conflicts of interest.

Appendix A. Supplementary data

Supplementary data to this article can be found online at https://doi.org/10.1016/j.bbrep.2021.101183.

References

[1] E.J. Benjamin, P. Muntner, A. Alonso, M.S. Bittencourt, C.W. Callaway, A. P. Carson, A.M. Chamberlain, A.R. Chang, S. Cheng, S.R. Das, F.N. Delling, L. Djousse, M.S.V. Elkind, J.F. Ferguson, M. Fornage, L.C. Jordan, S.S. Khan, B. M. Kissela, K.L. Knutson, T.W. Kwan, D.T. Lackland, T.T. Lewis, J.H. Lichtman, C. T. Longenecker, M.S. Loop, P.L. Lutsey, S.S. Martin, K. Matsushita, A.E. Moran, M. E. Mussolino, M. O'Flaherty, A. Pandey, A.M. Perak, W.D. Rosamond, G.A. Roth, U. K.A. Sampson, G.M. Satou, E.B. Schroeder, S.H. Shah, N.L. Spartano, A. Stokes, D. L. Tirschwell, C.W. Tsao, M.P. Turakhia, L.B. VanWagner, J.T. Wilkins, S.S. Wong, S.S. Virani, Heart disease and stroke statistics-2019 update: a report from the American heart association, Circulation 139 (2019) e56–e528, https://doi.org/10.1161/cir.0000000000000659.
[2] R.A. Byrne, M. Joner, A. Kastrati, Stent thrombosis and restenosis: what have we learned and where are we going? The Andreas Gruntzig Lecture ESC 2014, Eur. Heart J. 36 (2015) 3320–3331, https://doi.org/10.1093/eurheartj/ehv511.
[3] A.C. Newby, An overview of the vascular response to injury: a tribute to the late Russell Ross, Toxicol. Lett. 112–113 (2000) 519–529.
[4] Z. Tang, A. Wang, F. Yuan, Z. Yan, B. Liu, J.S. Chu, J.A. Helms, S. Li, Differentiation of multipotent vascular stem cells contributes to vascular diseases, Nat. Commun. 3 (2012) 875, https://doi.org/10.1038/ncomms1867.
[5] M.R. Bennett, S. Sinha, G.K. Owens, Vascular smooth muscle cells in atherosclerosis, Circ. Res. 118 (2016) 692–702, https://doi.org/10.1161/CIRCRESAHA.115.306361.
[6] P.S. Mathieu, E. Fitzpatrick, M. Di Luca, P.A. Cahill, C. Lally, Resident multipotent vascular stem cells exhibit amplitude dependent strain avoidance similar to that of vascular smooth muscle cells, Biochem. Biophys. Res. Commun. S0006–0291X (19) (2019), https://doi.org/10.1016/j.bbrc.2019.10.185, 32101-32101.
[7] S. Ghazanfari, A. Driessen-Mol, G.J. Strijkers, F.M. Kanters, F.P. Baaijens, C. V. Bouten, A comparative analysis of the collagen architecture in the carotid artery: second harmonic generation versus diffusion tensor imaging, Biochem. Biophys. Res. Commun. 426 (2012) 54–58, https://doi.org/10.1016/j.bbrc.2012.08.031.
[8] S. Sugita, T. Matsumoto, Heterogeneity of deformation of aortic wall at the microscopic level: contribution of heterogeneous distribution of collagen fibers in the wall, Bio Med. Mater. Eng. 23 (2013) 447–461, https://doi.org/10.3233/BME-130771.
[9] S.R. Watson, P. Liu, E.A. Pena, M.A. Sutton, J.F. Eberth, S.M. Lessner, Comparison of aortic collagen fiber angle distribution in mouse models of atherosclerosis using second-harmonic generation (SHG) microscopy, Microsc. Microanal. 22 (2016) 55–62, https://doi.org/10.1017/S1431927615015585.
[10] C. Pagiatakis, R. Galaz, J.C. Tardif, R. Mongrain, A comparison between the principal stress direction and collagen fiber orientation in coronary atherosclerotic plaque fibrous caps, Med. Biol. Eng. Comput. 53 (2015) 545–555, https://doi.org/10.1007/s11517-015-1257-z.
[11] S. Ghazanfari, A. Driessen-Mol, S.P. Hoerstrup, F.P. Baaijens, C.V. Bouten, Collagen matrix remodeling in stented pulmonary arteries after transapical heart valve replacement, Cells Tissues Organs 201 (2016) 159–169, https://doi.org/10.1159/000442521.

[12] H. Khilji, In-Vitro Effects of Intravascular Stenting on Collagen Fiber Reorientation and Tissue Remodeling (Master's thesis), 2017.

[13] C.M. Potter, K.H. Lao, L. Zeng, Q. Xu, Role of biomechanical forces in stem cell vascular lineage differentiation, Arterioscler. Thromb. Vasc. Biol. 34 (2014) 2184–2190, https://doi.org/10.1161/ATVBAHA.114.303423.

[14] E.M. Campbell, P.A. Cahill, C. Lally, Investigation of a small-diameter decellularised artery as a potential scaffold for vascular tissue engineering; biomechanical evaluation and preliminary cell seeding, J Mech Behav Biomed Mater 14 (2012) 130–142, https://doi.org/10.1016/j.jmbbm.2012.06.001.

[15] R.T. Gaul, D.R. Nolan, C. Lally, Collagen fibre characterisation in arterial tissue under load using SALS, J Mech Behav Biomed Mater 75 (2017) 359–368, https://doi.org/10.1016/j.jmbbm.2017.07.036.

[16] S.J. Aper, A.C. van Spreeuwel, M.C. van Turnhout, A.J. van der Linden, P. A. Pieters, N.L. van der Zon, S.L. de la Rambelje, C.V. Bouten, M. Merkx, Colorful protein-based fluorescent probes for collagen imaging, PLoS One 9 (2014), e114983, https://doi.org/10.1371/journal.pone.0114983.

[17] G.M. Fomovsky, J.W. Holmes, Evolution of scar structure, mechanics, and ventricular function after myocardial infarction in the rat, Am. J. Physiol. Heart Circ. Physiol. 298 (2010) H221–H228, https://doi.org/10.1152/ajpheart.00495.2009.

[18] J. Li, M. Wu, J. Chu, R. Sochol, S. Patel, Engineering micropatterned surfaces to modulate the function of vascular stem cells, Biochem. Biophys. Res. Commun. 444 (2014) 562–567, https://doi.org/10.1016/j.bbrc.2014.01.100.

[19] T. Boulesteix, A.M. Pena, N. Pages, G. Godeau, M.P. Sauviat, E. Beaurepaire, M. C. Schanne-Klein, Micrometer scale ex vivo multiphoton imaging of unstained arterial wall structure, Cytometry 69 (2006) 20–26, https://doi.org/10.1002/cyto.a.20196.

[20] G.R. Houtchens, M.D. Foster, T.A. Desai, E.F. Morgan, J.Y. Wong, Combined effects of microtopography and cyclic strain on vascular smooth muscle cell orientation, J. Biomech. 41 (2008) 762–769, https://doi.org/10.1016/j.jbiomech.2007.11.027.

[21] A. Colombo, S. Guha, J.N. Mackle, P.A. Cahill, C. Lally, Cyclic strain amplitude dictates the growth response of vascular smooth muscle cells in vitro: role in in-stent restenosis and inhibition with a sirolimus drug-eluting stent, Biomech. Model. Mechanobiol. 12 (2013) 671–683, https://doi.org/10.1007/s10237-012-0433-4.

[22] M.C. Weiser, R.A. Majack, A. Tucker, E.C. Orton, Static tension is associated with increased smooth muscle cell DNA synthesis in rat pulmonary arteries, Am. J. Physiol. 268 (1995) H1133–H1138, https://doi.org/10.1152/ajpheart.1995.268.3.H1133.

[23] D. Skowasch, A. Jabs, R. Andrie, S. Dinkelbach, B. Luderitz, G. Bauriedel, Presence of bone-marrow- and neural-crest-derived cells in intimal hyperplasia at the time of clinical in-stent restenosis, Cardiovasc. Res. 60 (2003) 684–691.

[24] A.J. Carter, J.R. Laird, A. Farb, W. Kufs, D.C. Wortham, R. Virmani, Morphologic characteristics of lesion formation and time course of smooth muscle cell proliferation in a porcine proliferative restenosis model, J. Am. Coll. Cardiol. 24 (1994) 1398–1405, https://doi.org/10.1016/0735-1097(94)90126-0.

[25] L.H. Timmins, M.W. Miller, F.J. Clubb Jr., J.E. Moore Jr., Increased artery wall stress post-stenting leads to greater intimal thickening, Lab. Invest. 91 (2011) 955–967, https://doi.org/10.1038/labinvest.2011.57.

[26] J.K. Park, K.S. Lim, I.H. Bae, J.P. Nam, J.H. Cho, C. Choi, J.W. Nah, M.H. Jeong, Stent linker effect in a porcine coronary restenosis model, J Mech Behav Biomed Mater 53 (2016) 68–77, https://doi.org/10.1016/j.jmbbm.2015.08.014.

[27] T.M. Sullivan, S.D. Ainsworth, E.M. Langan, S. Taylor, B. Snyder, D. Cull, J. Youkey, M. Laberge, Effect of endovascular stent strut geometry on vascular injury, myointimal hyperplasia, and restenosis, J. Vasc. Surg. 36 (2002) 143–149, https://doi.org/10.1067/mva.2002.122878.